Journal of Power Sources 245 (2014) 772–778

Contents lists available at SciVerse ScienceDirect

Journal of Power Sources

journal homepage: www.elsevier.com/locate/jpowsour

Metal free nitrogen doped hollow mesoporous graphene-analogous spheres as effective electrocatalyst for oxygen reduction reaction

Jing Yan [a], Hui Meng [b], Fangyan Xie [c], Xiaoli Yuan [a], Wendan Yu [a], Worong Lin [a], Wenpeng Ouyang [a], Dingsheng Yuan [a,*]

[a] Department of Chemistry, Jinan University, Guangzhou 510632, PR China
[b] Department of Physics and Siyuan Laboratory, College of Science and Engineering, Jinan University, Guangzhou 510632, PR China
[c] Instrumental Analysis & Research Center, Sun Yat-sen University, Guangzhou 510275, PR China

GRAPHICAL ABSTRACT

Nitrogen-doped hollow mesoporous carbon sphere (N-doped HMCS) composed by broken graphene was synthesized, the carbon spheres showed effective activity as electrocatalyst for the oxygen reduction reaction (ORR) in alkaline solution with unique methanol-tolerant property.

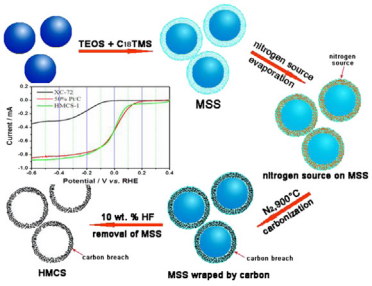

ARTICLE INFO

Article history:
Received 19 April 2013
Received in revised form
7 June 2013
Accepted 1 July 2013
Available online 9 July 2013

Keywords:
Hollow mesoporous carbon sphere
Nitrogen-doped carbon
Graphene
Oxygen reduction reaction
Fuel cell

ABSTRACT

Nitrogen-doped hollow mesoporous carbon spheres has been synthesized from mesoporous silica spheres using glycine as carbon and nitrogen precursor. The wall of the spheres is composed by broken graphene. The metal free nitrogen-doped hollow mesoporous carbon spheres are proven to be active electrocatalyst for the oxygen reduction reaction in alkaline solution. A unique advantage of the nitrogen-doped hollow mesoporous carbon sphere is its methanol-tolerant property because of the absence of active metal. The catalytic activity is ascribed to the pyridinic-nitrogen formed during pyrolysis and the graphene-like structure. To the best of our knowledge this is the first report on the nitrogen-doped hollow mesoporous carbon sphere as a metal-free electrocatalyst for the oxygen reduction reaction which is an important reaction in fuel cell. The prepared mesoporous carbon material can also be used as catalyst support and find application both in the anode and cathode of fuel cell.

1. Introduction

Fuel cells convert chemical energy directly into electrical current without combustion and they are attractive power sources for portable, automotive and stationary applications due to high energy density and efficiency. However the low kinetics of cathodic oxygen reduction reaction (ORR) causes a big loss in the efficiency [1]. Pt is a typical catalyst for ORR due to its high activity and stability. However, the high price and limited supply of Pt poses serious problems to the commercialization of fuel cell [2]. In addition, Pt-based catalyst is susceptible to time-dependent drift

* Corresponding author.
E-mail addresses: tmh@jnu.edu.cn (H. Meng), tydsh@jnu.edu.cn (D. Yuan).

0378-7753/$ – see front matter © 2013 Published by Elsevier B.V.
http://dx.doi.org/10.1016/j.jpowsour.2013.07.003

and the crossover of methanol causes mixed potential in the cathode [3–5]. Thus, research efforts in the development of cathode catalyst have been focused on decreasing Pt content or replacing Pt with less expensive materials. Noble metal free catalyst for the ORR became a hot topic and lots of progress has been made [4,6].

Recently nitrogen-doped carbon nanostructures (NCNS) were found to be active for ORR [7–13]. The origin of the activity was explained by the presence of pyridinic nitrogen [8,9]. Various synthesis methods for NCNS have been reported in literature, such as post synthesis modification [14–16], chemical vapor deposition [17,18], and liquid impregnation [19]. The structure of the nitrogen-doped carbon materials were usually ordered mesoporous carbon, carbon nanotubes, carbon nanowires, graphene, and so on. These materials exhibited high ORR activity, however, their mass production was limited by the complexity of the synthesis process. For practical application in fuel cells, it is required to develop cheap material that is possible for mass production.

In this study, nitrogen-doped hollow mesoporous carbon spheres (HMCS) was synthesized via a simple liquid impregnation method using mesoporous silica spheres as template and cheap glycine as carbon and nitrogen precursor. The HMCS was used as metal-free ORR catalyst and exhibited excellent activity with direct four electron process and methanol-tolerant behavior. The cathode ORR reaction is a bottleneck for the mass commercialization of fuel cell because the low kinetics of ORR requires much more catalyst than anode. The activity of HMCS was inferior to the commercial Pt/C catalyst, there are several strategies to improve the activity which is still going on, but considering the cost and the potential improvement the HMCS was promising candidate as ORR catalyst.

2. Experimental

2.1. Synthesis of submicrometer-sized mesoporous silica spheres (MSS)

In a typical synthesis, 3.5 ml aqueous ammonia (30 wt. %) was added into a solution containing 75 ml ethanol and 10 ml ultrapure water. After stirring for 15 min, 5 ml tetraethylorthosilicate (TEOS) (98 wt. %) was added at 30 °C under vigorous stirring, and the mixture was stirred for 6 h to yield uniform silica spheres.

A mixture containing 5 ml TEOS and 2 ml trimethoxy(octadecyl) silane (C_{18}TMS) (90 wt. %) was added into the colloidal solution containing silica spheres and further reacted for 1 h. The final material was retrieved by centrifugation and further calcined at 550 °C for 6 h under oxygen atmosphere.

2.2. Synthesis of nitrogen-doped hollow mesoporous carbon sphere (HMCS)

0.1 g MSS was added to a mixture of 0.5 g glycine and 50 g H_2O. The mixture was ultrasonicated at 30 °C for 30 min to get pale yellow mixture, which was transferred into a Teflon-lined autoclave, the autoclave was sealed and kept at 180 °C overnight in an electric oven. After the autoclave was cooled down to room temperature naturally, the pale yellow emulsion was transferred into a beaker and stirred at 70 °C, until the emulsion became dry and an orange solid was obtained, in this process the internal pores of MSS were completely infiltrated with carbon source. The as-prepared dry mixtures was heat treated at 300 °C for 20 min, and then increased to 900 °C and maintained for another 3 h for carbonization. This process was under pure N_2 atmosphere with the heating rate of 2 °C min^{-1} and the cooling rate of 5 °C min^{-1} to room temperature. Then the carbon-silica composite was washed in 10 wt. % HF solution overnight to completely remove the silica template. The final product was labeled as HMCS-1.

In parallel experiments glycine was changed into L-lysine or glucose and the products were labeled as HMCS-2 and HMCS-3. HMCS-2 and HMCS-1 were of different nitrogen source and HMCS-3 had no nitrogen.

2.3. Physical characterization

The samples were characterized by a MSAL-XD2 X-ray diffractometer (XRD, Cu Ka, 40 kV, 20 mA, $\lambda = 1.54056$ Å). The fourier-transformed infrared spectra (FT-IR) measurements were conducted on a Nicolet 6700 FT-IR spectrometer by using pressed KBr pellets. The morphology was observed via a Philips TECNAI-10 transmission electron microscope (TEM) using an accelerating voltage of 100 kV and JEM2010 high-resolution transmission electron microscopy (HRTEM) operating at 200 kV. The crystallization degree of HMCS was investigated by Raman spectroscopy, which was recorded in a backscattering configuration using the 514.5 nm Ar^+ ion laser and a Renishaw Raman spectrometer. The X-ray photoelectronic spectroscopy (XPS) was carried out using an ESCALab250 spectrometer with Alumina Ka (1486.6 eV) source. Nitrogen sorption isotherms of as-prepared materials were studied by a Micromertics TriStar 3000 analyzer at 77 K. The plot of specific surface area was deduced from the isotherm analysis of adsorption data at the relative pressure (P/P_0) of 0–1.0 and the average pore diameters were collected from the peak value on the pore diameter distribution.

2.4. Electrochemical characterization

The electrochemical measurements were carried out on potentiostat (CHI 660D, CH Instruments, Inc.) at 25 C in a conventional three-electrode system. Platinum foil (1.0×1.0 cm^2) and Ag/AgCl (saturated KCl) were used as counter electrode and reference electrode, respectively. The potential was converted to versus reversal hydrogen electrode (RHE) for parallel comparison with literature values. A rotating disk electrode (RDE) system was used as working electrode, the glassy carbon electrode (5 mm diameter) was polished before each experiment with 1, 0.3 and 0.05 mm alumina power, respectively, and then washed in a mixture of ethanol and water before each experiment. The ORR activity of HMCS was evaluated in 0.1 M KOH solution and recorded with the potentiostat at a scan rate of 10 mV s^{-1}. To make KOH solution oxygen or nitrogen saturated, pure O_2 or pure N_2 gas was bubbled directly into the solution for at least 30 min before measurements and was flushed over the cell solution during the tests.

All the working electrodes were prepared with the same procedure as follows: 2 mg catalyst was put into 1 ml ethanol solution containing 100 μl Nafion (5 wt. %). The mixture was sonicated for 30 min, and 5 μl or 10 μl of the dispersion was deposited on the glassy carbon electrode and dried under ambient conditions.

3. Results and discussion

3.1. Formation mechanism of the HMCS

The HMCS was designed to be hollow carbon spheres according to the preparation procedure shown in Fig. 1. Silica spheres were used as template, the surface of which was covered by a layer of mesoporous structure (MSS). Under controlled reaction conditions the mesoporous layer of MSS was filled with nitrogen and carbon precursor. The precursor was carbonized at high temperature, forming a carbon layer over the silica core. The nitrogen element in the precursor was left in the carbon cover. The carbon layer was

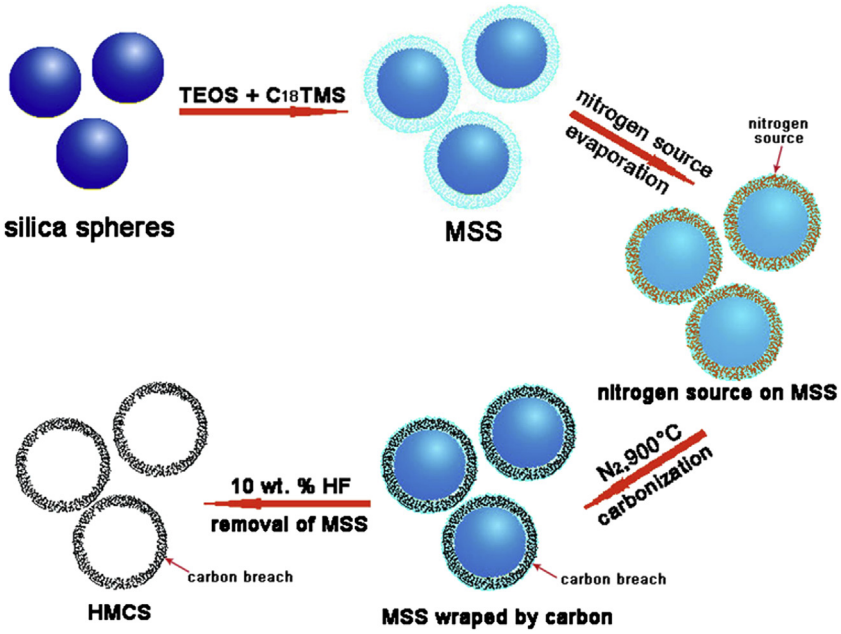

Fig. 1. Schematic illustration of the formation of HMCS.

mesoporous with lots of breach, which made the removal of inner silica possible. The final product was hollow mesoporous carbon spheres (HMCS) with breach inside the wall. The hollow structure was favorable because the active sites were expected to be dispersed uniformly on both the inner and outer wall of the carbon spheres, which would make the best use of the active elements and lead to high performance.

3.2. Morphology and crystalline characterization of HMCS

Following the mechanism described above, the HMCS was designed to be hollow carbon spheres. However TEM micrographs revealed different structures for the two different precursors. As shown in Fig. 2a and b, when glycine was used as precursor a kind of hollow carbon sphere structure was prepared, while with L-lysine as precursor all the spheres were broken. Considering that all other conditions and procedures were the same, the difference could only be explained by the precursor. In the preparation procedure a key step was the carbonization of the nitrogen precursor filled MSS, in this step the macromolecular turned into carbon and nitrogen was left. At the high temperature of carbonization glycine and L-lysine would melt first, the difference of viscosity and the interaction with the carbon surface of the melted precursor determined the dispersion. L-lysine has longer carbon chain than glycine, which makes melted L-lysine less hydrophilic to the surface of silica. The melted glycine remained where it was while the melted L-lysine flowed down along the wall of the carbon sphere and accumulated at the bottom, leaving the upper side of the MSS no precursor. In the carbonization process carbon was formed only at the bottom, forming the hemi-spheres and broken spheres as shown in Fig. 2b. While the melted glycine was filled uniformly inside the surface of MSS, after carbonization a perfect carbon layer was formed on the MSS. After the removal of the inner silica the hollow carbon sphere was formed as shown in Fig. 2a. As catalyst for electro-catalytic reaction the hollow carbon structure was more favorable because in the hollow sphere the active sites were dispersed uniformly while in the broken spheres some of the active sites were covered inside the wall and not exposed. The predicted performance in the ORR was confirmed by following electrochemical characterizations. Enlarged TEM in Fig. 2c gave more details of the hollow carbon sphere HMCS-1, most of the carbon spheres were spherical and uniform with an average particle size of about 180 nm and shell thickness of 20 nm. No obvious lattice-fringe images could be observed in the HRTEM micrograph of HMCS-1 in Fig. 2d, which meant the carbon was not graphitized. Fragment of graphene could be observed in Fig. 2d, implying the wall of the HMCS was composed by broken graphene. The selected area electron diffraction (SAED) inserted in Fig. 2d also proved above conclusion because the appearance of circles of confusion instead of lattice diagram. The X-ray diffraction (XRD) patterns in Fig. S1 (see support materials) also support above conclusion. Two broad diffraction peaks appeared at 2θ of 24 and 44, corresponding to the (002) facet of disordered carbon phase and (101) facet of graphitized carbon [20]. The intensity of the graphite peak was negligible compared with the disordered peak, suggesting that the sample was amorphous carbon.

3.3. Specific surface area and pore size of HMCS

Nitrogen adsorption–desorption isotherms and the derived pore size distribution of HMCS-1 and MSS were plotted in Fig. 3. The prepared material was abundant with mesopores and micropores, which was proven by the pseudo-type-I isotherm with H1 hysteresis loop at high relative pressure [20]. The adsorption of micropores took place at low relative pressure where the adsorption isotherm of the sample became rapidly saturated. The platform at $P/P_0 = 0.20–0.70$ originated from the outer surface adsorption of the shell of the sphere. There was a clear increase from a relative pressure of 0.8 in the adsorption branch of HMCS-1 and a hysteresis loop at $P/P_0 = 0.80–0.99$ with a pronounced desorption step, demonstrating macroporous adsorption of the carbon sphere. The macropores could be observed in the HRTEM image. Brunauer–Emmett–Teller (BET) measurements were used to get the specific surface area of HMCS-1 and MSS. High specific surface area (451 $m^2\ g^{-1}$) of HMCS-1 was get compared with 335 $m^2\ g^{-1}$ for MSS. The increased specific surface area was contributed by the mesoporous structure of the hollow carbon shell. With the same method the specific surface area of HMCS-2 and HMCS-3 were

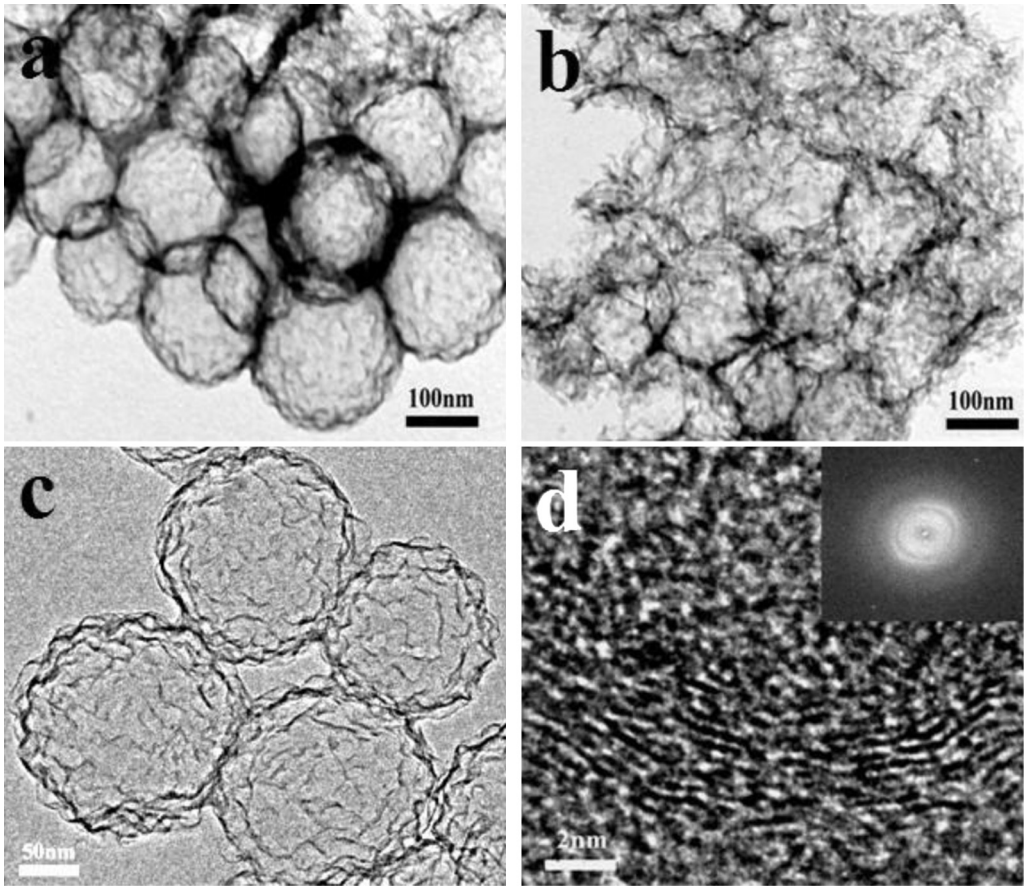

Fig. 2. TEM micrographs of HMCS-1 (a) and HMCS-2 (b); HRTEM micrographs (c and d) and SAED (inset in d) of HMCS-1.

calculated to be 469 and 381 $m^2\ g^{-1}$ as shown in Fig. S2. The higher specific surface area of HMCS-2 was explained by the structure of broken spheres. The pore size distribution plots in Fig. 3b. It was observed that uniform pore size distribution centered at around 3 nm for HMCS-1 and 4 nm of MSS. The total pore volumes of HMCS-1 and MSS were 1.16 and 0.303 $cm^3\ g^{-1}$, respectively.

3.4. Raman characterization of HMCS

Raman spectroscopy is a convenient tool for characterizing carbon materials. Raman spectroscopy of HMCS was given in Fig. 4. Both HMCS-1 and HMCS-2 exhibited two peaks at around 1340 and 1590 cm^{-1}. The D peak (1340 cm^{-1}) corresponds to modes associated with transverse optical phonons around the edge of the Brillouin zone. In the molecular picture, it is associated with the breathing mode of the sp [2] aromatic rings. The D peak is usually very intense in amorphous carbon samples, while it is absent in perfect graphitic samples. The G peak (1580 cm^{-1}) corresponds to doubly degenerate E_{2g} mode at the Brillouin zone center. In the molecular picture of carbon materials, the G peak is due to the bond stretching of all pairs of sp^2 atoms. Usually the D peak was assigned to the disordered carbon and the G band was referred to graphite band of carbon. The I_D/I_G ratio is a factor for judging the degree of graphitization of carbon. The I_D/I_G ratios determined from integrated peak area of HMCS-

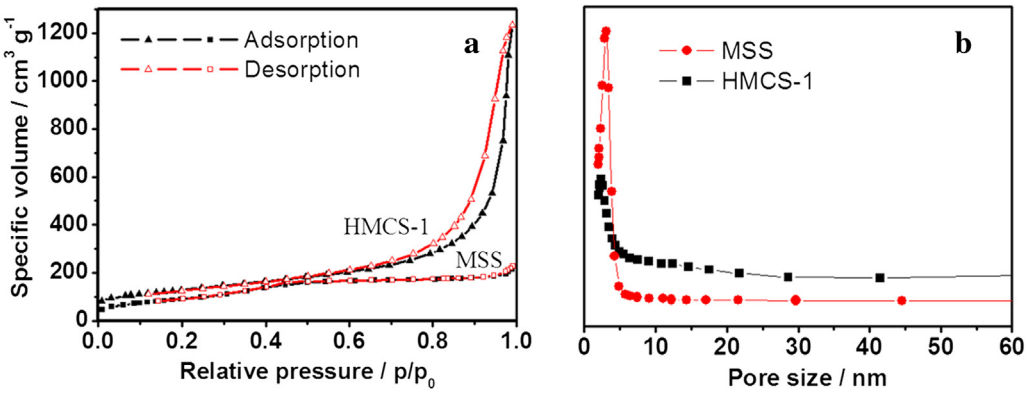

Fig. 3. N_2 adsorption–desorption isotherms of HMCS-1 (a) and pore size distribution (b).

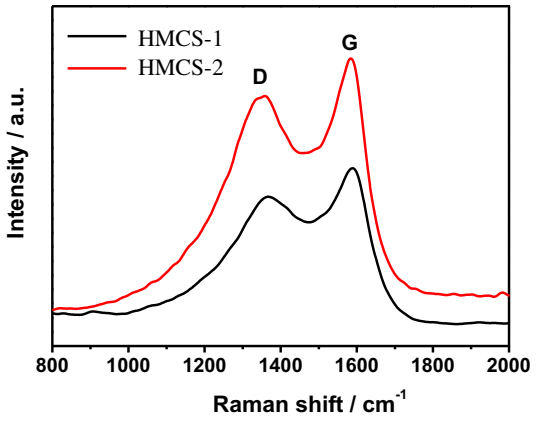

Fig. 4. Raman spectra of HMCS-1 and HMCS-2.

1 and HMCS-2 were 1.24 and 1.23, which was the same of the bi-layer graphene [21,22]. Going back to HRTEM in Fig. 2d, interrupted graphene layers could be observed in the wall of the hollow carbon spheres. It was concluded that the synthesized carbon material was analogous graphene. Other characterizations such as TEM, SAED and XRD all proved the amorphous nature of the material. This was because the graphene was broken and macroscopically the material did not show the graphitic nature of graphene.

3.5. Elemental analysis of HMCS

Since the synthesized carbon material was nitrogen-doped, it was vital to determine the chemical state and content of nitrogen in the material which would directly influence the electrochemical performance [23,24]. X-ray photoelectron spectroscopy (XPS) was employed to identify the surface nitrogen content and the chemical states of nitrogen. As shown in Fig. 5a was the XPS survey spectrum of HMCS-1 and HMCS-2, showing C1s, N1s and O1s peaks. The N1s peak in the survey spectrum proved the existence of the nitrogen element in both HMCS-1 and HMCS-2. Detailed analysis of C1s and N1s peaks were shown in Fig. 5b and c. The overlapped C1s peaks were decomposed into four components arising from C–C (284.5 eV), C–N (285.6 eV), C–O (286.3 eV) and C=O (287.2 eV). The first peak was usually attributed to the sp^2 hybridized carbon. The second was originated from the interaction between carbon and nitrogen, implying the existence of interaction between carbon and nitrogen. The peaks centered around 286.3 eV and 287.2 eV were interpreted as the sp^2 and sp^3 hybridized carbon bonded to sp^2 and sp^3 hybridized oxygen, respectively [17,25]. Four types of nitrogen were recognized from N1s spectrum in Fig. 5c which were located at 398.4 eV, 400.1 eV, 401.2 eV and 403.4 eV, corresponding to the pyridinic-N(N-6), pyrrolic-N(N-5), quaternary-N(N–Q) and pyridinic-N-oxide (N-oxide) groups [26,27].

The total nitrogen contents of HMCS-1 and HMCS-2 were calculated from XPS to be 3.82 and 3.05 wt%. Detailed analysis from the XPS spectrum in Fig. 5c indicated high percentage of pyridinic-N and quaternary-N. The content of the pyridinic-N in HMCS-1 was 33.4 wt%, which was higher than HMCS-2 (25.0 wt%). The content of pyrrolic-N in HMCS-1 was 12.3 wt%, also higher than HMCS-2 (7.6 wt%). While the content quaternary-N was opposite: 41.8 wt% for HMCS-1 and 59.8 wt% for HMCS-2. It was commonly accepted that the ORR activity of nitrogen-doped carbon came from the pyridinic-N and pyrrolic-N [12,28,29]. Since HMCS-1 had more

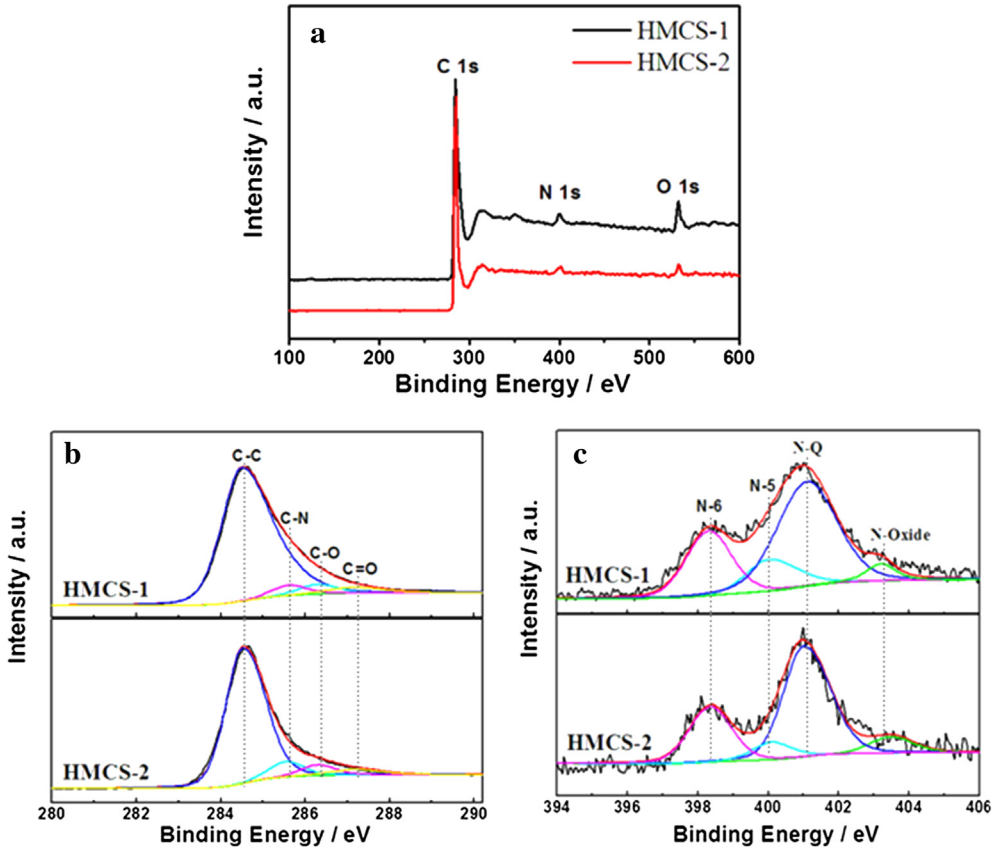

Fig. 5. XPS survey spectra (a), High-resolution XPS spectra of C1s (b) and N1s (c) of the HMCS-1 and HMCS-2.

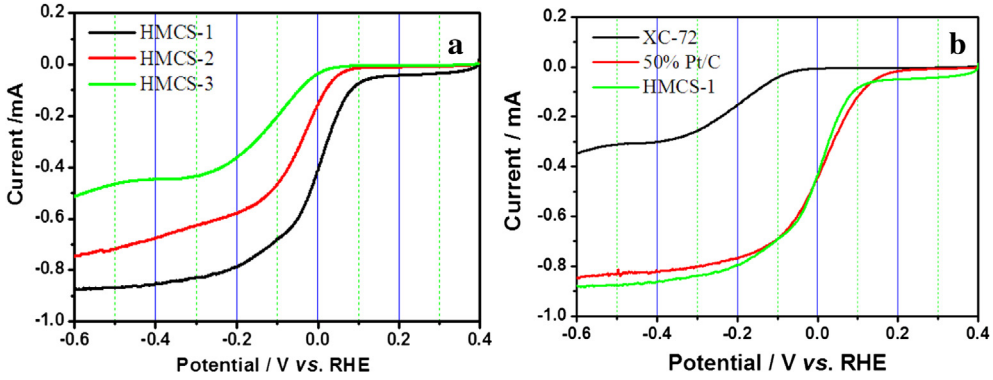

Fig. 6. ORR polarization curves of HMCS in O_2 saturated 0.1 M KOH solution with RDE, sweep rate: 10 mV s^{-1}, rotation speed: 1600 rpm.

pyridinic-N than HMCS-2, it was predicted to have better performance in ORR.

3.6. Electrochemical characterization of HMCS

The activities of HMCS for oxygen electroreduction in O_2-saturated 0.1 M KOH electrolyte were evaluated as shown in Fig. 6. Compared with nitrogen-free HMCS-3, HMCS-1 and HMCS-2 showed obvious activity for ORR. The limit current of HMCS-3 only reached 0.44 mA and the onset potential of ORR was 0 V versus reversal hydrogen electrode (RHE) which was typical performance of carbon powder for ORR [30,31]. When the carbon material was doped with nitrogen there appeared obvious improvements in ORR activity. Comparing HMCS-1 and HMCS-2, the onset potential of HMCS-1 was 50 mV positive than HMCS-2 (0.14 V and 0.08 V versus RHE for HMCS-1 and HMCS-2, respectively), the limit current of HMCS-1 reached 0.87 mA. The improved performance of HMCS-1 compared with HMCS-2 was explained by two factors: more pyridinic-N and the hollow structure made more nitrogen available in the reaction. Fig. 6b compared the performance of HMCS-1, commercial Vulcan XC-72 carbon powder and commercial 50% Pt/C catalyst. It was noteworthy to find similar performance of HMCS-1 with Pt/C catalyst. Both catalysts had similar limit current and the onset potential of Pt/C catalyst was 60 mV positive than HMCS-1 which proves the present system still cannot compete with Pt/C. But considering the totally free of Pt in HMCS-1, these values were among the best reported in literature. The performance of Vulcan XC72 carbon was similar with that of HMCS-3, which was common for carbon materials without nitrogen. It was concluded that doping carbon with nitrogen could make the material active for ORR in alkaline solution, the activity was to some degree determined by the content of the pyridinic-N, and the graphene like structure of the carbon sphere would also contribute to the high performance.

There were two possible mechanism of ORR on different catalysts: the two electron pathway and the direct four electron pathway. The four electron pathway was favorable in fuel cells because it offered higher kinetics of ORR. It was recognized that ORR took place via the four electron pathway on Pt/C catalyst. The number of electrons transferred on the HMCS-1 catalyst was calculated according to the Koutecký–Levich equation as shown in Fig. 7 [32,33].

$$1/j_{\mathrm{lim}} = 1/j_{\mathrm{lev}} + 1/j_{\mathrm{k}} = 1/\left(B\omega^{1/2}\right) + 1/j_{\mathrm{k}} \quad (1)$$

$$B = 0.62nFC_{\mathrm{O}}(D_{\mathrm{O}})^{2/3}\nu^{-1/6} \quad (2)$$

$$j_k = nFkC_{\mathrm{O}} \quad (3)$$

where the j_{lim} (mA cm^{-2}) is the measured current density, which is related to Levich current (j_{lev}) and kinetic current (j_{k}). F is the Faraday constant (96486.4 C mol^{-1}), D_{O} is the diffusion coefficient of oxygen in 0.1 M KOH (1.9×10^{-5} cm^2 s^{-1}), ν is the kinematic viscosity of the water (0.01 cm^2 s^{-1}), C_{O} is the bulk concentration of oxygen in air-saturated 0.1 M KOH (1.21×10^{-6} mol cm^{-3}). And ω is the rotation rate of RDE, n is the electron transfer numbers of ORR. The linear plot of j_{lim}^{-1} versus $\omega^{-1/2}$ has a slope of $1/0.62nFCD^{2/3}\nu^{-1/6}$ (Fig. 7b). The constant 0.62 is adopted when the rotation speed is expressed in rpm. On the basis of the line slopes,

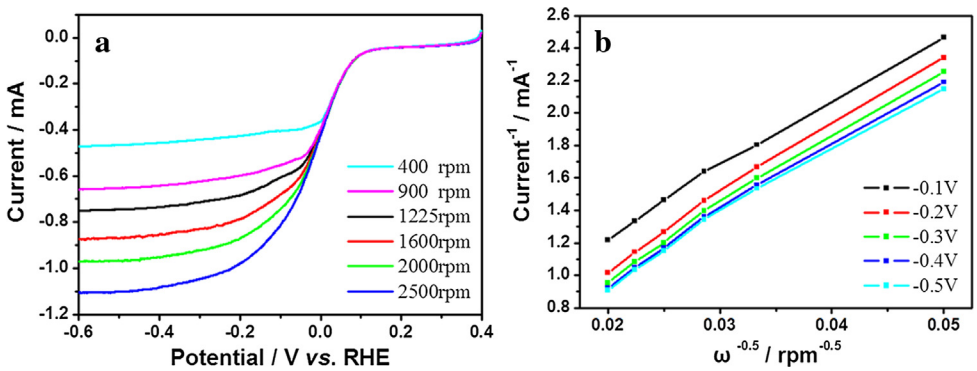

Fig. 7. (a) ORR polarization curves of HMCS-1 at different rotating speeds in 0.1 M KOH solution saturated with O_2. Scan rate: 10 mV s^{-1}. (b) Koutecký–Levich plot of j_{lim}^{-1} vs. $\omega^{-1/2}$ obtained at −0.3, −0.4, −0.5, −0.6 and −0.7 V.

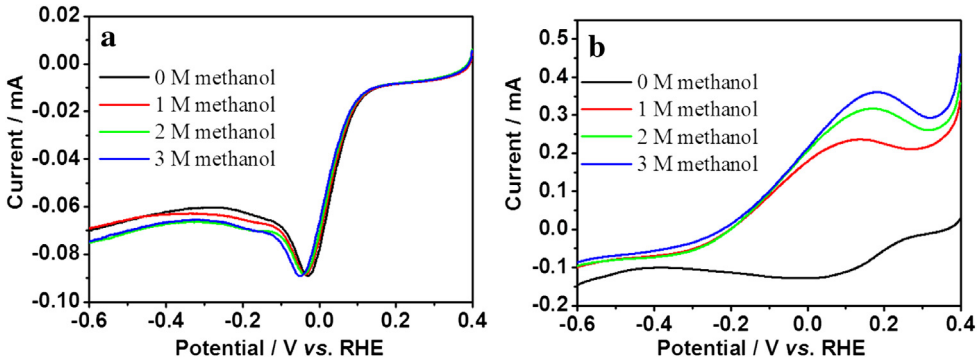

Fig. 8. Steady state polarization curves of ORR in O_2 saturated 0.1 M KOH with different concentration of methanol on HMCS-1 (a) and commercial 50% Pt/C catalyst (b).

a n value of 3.9 was obtained in the potential range of −0.3 to −0.7 V. The results indicated that the ORR on HMCS-1 was a four electron reaction, which was the same with Pt/C catalyst, proving HMCS-1 a promising metal-free efficient ORR catalyst in alkaline solution.

The crossover of methanol from anode to cathode in direct methanol fuel cells was one of the challenges to overcome in direct methanol fuel cells. The usually used cathode catalyst, such as the Pt group metal, was also active in the oxidation of methanol, thus causing mixed cathode potential and greatly reduced the efficiency of fuel cell. So the cathode catalyst was required to have no activity in methanol oxidation while active in ORR. The Pt group catalyst could not meet this requirement. As shown in Fig. 8b, the addition of methanol into the electrolyte caused obvious mixed reaction. While methanol had no influence on the ORR of HMCS-1, there was almost no change in the polarization curves with and without methanol in Fig. 8a. The methanol-tolerant property of HMCS-1 showed its potential application in direct methanol fuel cells.

4. Conclusions

A kind of metal free nitrogen-doped carbon material (HMCS-1) was synthesized via a liquid impregnation method, using glycine as carbon and nitrogen source. The prepared material was composed by hollow spheres of high mesoporosity and large pore volume. HMCS-1 displayed comparable although inferior ORR activity with commercial Pt/C catalyst and excellent methanol tolerant ability. The ORR activity of the nitrogen-doped carbon was proved to originate from the pyridinic-N. The content and the availability of pyridinic-N and the graphene-like structure of the carbon material were vital factors determining the ORR activity. Subsequent work is the application of HMCS-1 in a membrane electrode assembly (MEA) with alkaline membrane and full cell test, which is underway.

Acknowledgments

This work was supported by National Natural Science Foundation of China (21031001 and 21106190), Program of the Pearl River Young Talents of Science and Technology in Guangzhou, China (2013055), Scientific Research Foundation for the Returned Overseas Chinese Scholars, State Education Ministry and Key Laboratory of Functional Inorganic Material Chemistry (Heilongjiang University), Ministry of Education.

Appendix A. Supplementary data

Supplementary data related to this article can be found at http://dx.doi.org/10.1016/j.jpowsour.2013.07.003.

References

[1] D. Su, G. Sun, Angew. Chem. Int. Ed. 50 (2011) 11570.
[2] C. Yang, Energy Policy 37 (2009) 1805.
[3] K. Gong, F. Du, Z. Xia, M. Durstock, L. Dai, Science 323 (2009) 760.
[4] M. Lefevre, E. Proietti, F. Jaouen, J.P. Dodelet, Science 324 (2009) 71.
[5] G. Wu, K.L. More, C.M. Johnston, P. Zelenay, Science 332 (2011) 443.
[6] E. Proietti, F. Jaouen, M. Lefèvre, N. Larouche, J. Tian, J. Herranz, J.P. Dodelet, Nat. Commun. 2 (2011) 416.
[7] R. Bashyam, P. Zelenay, Nature 443 (2006) 63.
[8] J. Ozaki, S. Tanifuji, A. Furuichi, K. Yabutsuka, Electrochim. Acta 55 (2010) 1864.
[9] V. Nallathambi, J.W. Lee, S.P. Kumaraguru, G. Wu, B.N. Popov, J. Power Sources 183 (2008) 34.
[10] G. Liu, X. Li, B.N. Popov, ECS Trans. 25 (2009) 1251.
[11] S.M. Lyth, Y. Nabae, S. Moriya, S. Kuroki, M. Kakimoto, J. Ozaki, S. Miyata, J. Phys. Chem. C 113 (2009) 20148.
[12] J.I. Ozaki, S.I. Tanifuji, N. Kimura, A. Furuichi, A. Oya, Carbon 44 (2006) 1324.
[13] A. Janosevic, I. Pasti, N. Gavrilov, S. Mentus, G. Ciric-Marjanovic, J. Krstic, J. Stejskal, Synth. Met. 161 (2011) 2179.
[14] J. Li, M.J. Vergne, E.D. Mowles, W. Zhong, D.M. Hercules, C.M. Lukehart, Carbon 43 (2005) 2883.
[15] E.N. Konyushenko, J. Stejskal, M. Trchová, J. Hradil, J. Kovárová, J. Prokes, M. Cieslar, J. Hwang, K. Chen, I. Sapurina, Polymer 47 (2006) 5715.
[16] T. Ramanathan, F.T. Fisher, R.S. Ruoff, L.C. Brinson, Chem. Mater. 17 (2005) 1290.
[17] L. Qu, Y. Liu, J.-B. Baek, L. Dai, ACS Nano 4 (2010) 1321.
[18] K.S. Kim, Y. Zhao, H. Jang, S.Y. Lee, J.M. Kim, K.S. Kim, J.H. Ahn, P. Kim, J.Y. Choi, B.H. Hong, Nature 457 (2009) 706.
[19] J. Zeng, C. Francia, C. Gerbaldi, M.A. Dumitresca, S. Specchia, P.J. Spinelli, Solid State Electrochem. 16 (2012) 3087.
[20] D. Yuan, T. Zhou, S. Zhou, W. Zou, S. Mo, N. Xia, Electrochem. Commun. 13 (2011) 242.
[21] C.S. Lee, L. Baraton, Z. He, J.L. Maurice, M. Chaigneau, D. Pribat, C.S. Cojocaru, Proc. SPIE 7761 (2010) 77610.
[22] A. Jorio, M.M. Lucchese, F. Stavale, E.H.M. Ferreira, M.V.O. Moutinho, R.B. Capaz, C.A. Achete, J. Phys. Condens. Matter 22 (2010) 334204.
[23] S. Maldonado, K.J. Stevenson, J. Phys. Chem. B 108 (2004) 11375.
[24] Y. Tang, B.L. Allen, D.R. Kauffman, A. Star, J. Am. Chem. Soc. 131 (2009) 13200.
[25] N. Gavrilov, I.A. Pasti, M. Mitric, J. Travas-Sejdic, G. Ciric-Marjanovic, S.V. Mentus, J. Power Sources 220 (2012) 306.
[26] S. Chen, J. Bi, Y. Zhao, L. Yang, C. Zhang, Y. Ma, Q. Wu, X. Wang, Z. Hu, Adv. Mater. 24 (2012) 5593.
[27] T. Sharifi, G. Hu, X. Jia, T. Wagberg, ACS Nano 10 (2012) 8904.
[28] T.C. Nagaiah, S. Kundu, M. Bron, M. Muhler, W. Schuhmann, Electrochem. Commun. 12 (2010) 338.
[29] N. Gavrilov, M. Vujkovic, I.A. Pasti, G. Ciric-Marjanovic, S.V. Mentus, Electrochim. Acta 56 (2011) 9197.
[30] S. Yang, K. Chang, Y. Huang, Y.F. Lee, H.W. Tien, S. Li, Y.H. Lee, C. Liu, C. Ma, C. Hu, Electrochem. Commun. 14 (2012) 39.
[31] D.S. Yu, E. Nagelli, F. Du, L.M. Dai, J. Phys. Chem. Lett. 1 (2010) 2165.
[32] I.Y. Jeon, D. Yu, S.Y. Bae, H.J. Choi, D.W. Chang, L. Dai, J.-B. Baek, Chem. Mater. 23 (2011) 3987.
[33] H. Meng, P.K. Shen, Electrochem. Commun. 8 (2006) 588.